Title
A Power Efficient Active Integrated Antenna Using Zeroth Order Antenna

Author
Lee, Joungyoung

Publication Date
2012

Peer reviewed|Thesis/dissertation

UNIVERSITY OF CALIFORNIA

Los Angeles

A Power Efficient Active Integrated Antenna Using Zeroth Order Antenna

A thesis submitted in partial satisfaction
of the requirements for the degree Master of Science
in Electrical Engineering

by

Joungyoung Lee

2012

ABSTRACT OF THE THESIS

A Power Efficient Active Integrated Antenna Using Zeroth Order Antenna

by

Joungyoung Lee

Master of Science in Electrical Engineering

University of California, Los Angeles, 2012

Professor Tatsuo Itoh, Chair

A microwave oscillator is integrated with a zeroth order resonance (ZOR) antenna to build an active oscillating antenna using the coplanar waveguide (CPW) technology. In this thesis, the basic metamaterial concept is introduced to understand the ZOR antenna and negative resistance method is also introduced to explain the design procedure of the oscillator type active integrated antenna (AIA). The CPW technology is utilized to design the entire circuit. The CPW TL gives a lot of advantages such as fabrication simplicity and design freedom. The ZOR antenna is utilized due to its electrically small size and high Q-factor which results in good phase noise of -92.5dBc/Hz at 100kHz offset. The proposed AIA is designed to achieve high DC-RF power conversion efficiency by suppressing higher order harmonic power. As a result, the radiated power of 14.57dBm (28.64mW) and the effective isotropic radiated power of (EIRP) 16.11dBm (40.83mW) is obtained with high DC to RF efficiency (27.2%), which is much higher than other active oscillator type AIA designs.

The thesis of Joungyoung Lee is approved.

M. C. Frank Chang

Y. Ethan Wang

Tatsuo Itoh, Committee Chair

University of California, Los Angeles

2012

Dedication

My beloved parents and sister

Contents

List of Figures

Acknowledgements

First and foremost, I would like to show my sincere gratitude to my advisor, Professor Tatsuo Itoh, for his guidance and advice. Also, I would like to thank my lab-colleagues, Jim Sun, Yuandan Dong, Han-sung Lee, Brandon Choi, Philip Hong, and Michael Wu, for their comments and help. Moreover, I would like to express my gratitude to my committee members, Professor M. C. Frank Chang, Professor Y. Ethan Wang, and Professor Tatsuo Itoh, for being my committee and offering their precious time and comments. Lastly, I would like to thank my family who dedicated their time and power to supporting me. Without all these people, I cannot possibly finish my MS thesis.

Chapter 1

Introduction

Active integrated antenna (AIA) has been received a growing attention in recent years, as we required new solution for high transmission-line loss, limited source power, and reduced antenna efficiency in modern millimeter-wave systems [1] [2]. The AIA is basically consisted of both an passive antenna and active circuitry. As an antenna designer's point of view, the AIA can be considered as an antenna that has built-in signal and wave processing capabilities such as mixing and amplification. However, As a microwave engineer's point of view, the AIA is an active microwave circuit that possesses the free space spatial input port and output port instead of a conventional 50Ohm transmission line. Also, at this point of view, the AIA is regarded as an element that provides many circuit functions such as radiating, resonating, diplexing, and filtering.

In the past, the AIA concept was used for designing of quasi optical mixers with an advantage of reducing the lossy and bulky interconnect between the device and antenna [3]. Also, by implementing the active devices in passive radiating elements, the AIA concept was employed with more advantages such as increasing the effective length of short antenna,

increasing antenna bandwidth, decreasing the mutual coupling between array elements, and improving the noise factor [4]. Recently, the AIA research has been focused on the area of efficient quasi-optical power combiners, also called spatial power combiner [5]. The Fig. 1.1 shows the oscillating AIA array application for power-combining and beam-scanning. This technology was originally proposed in order to combine the output power from an array of many solid-state devices in free space. By doing so, the combiner can overcome power loss limitations, which are so important in millimeter-wave frequency system [6] [7].

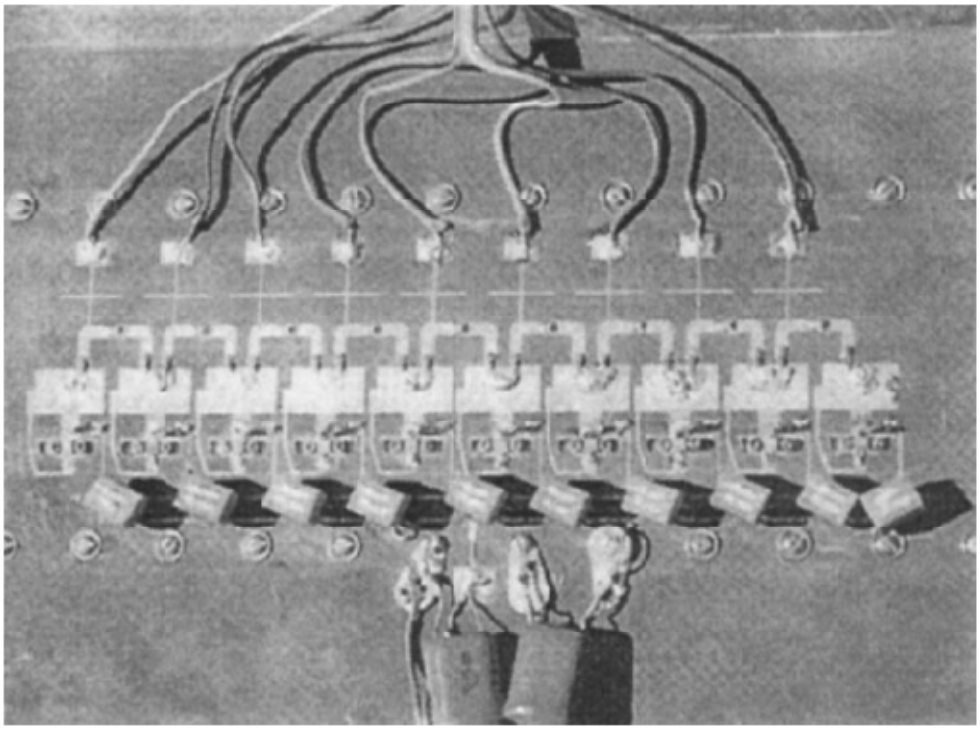

Figure 1.1: Photograph of a ten-element power-combining and beam-scanning array using coupled voltage controlled oscillator (VCO)'s

In past a few years, oscillator type AIA received much more attention than amplifier type AIA because of the requirement of compact, and high power sources for spatial power combiner application at millimeter wave frequencies [8] [9] [10]. Many innovative oscillator

type AIA design is proposed and successfully demonstrated for spatial power combiner application. As a source element of the AIA design, three terminal devices such as field-effect transistors (FETs) is commonly used over two terminal device because the FETs have higher efficiencies and lower noise figures than either Impatt or Gunn diodes. As a radiating element of the AIA design, patch antenna is typically used as shown in Fig 1.2. However, since the patch antenna is not satisfied the needs of the AIA such as compact size, high DC - radiated RF conversion efficiency, and good phase noise performance, the AIA research has been developed in order to satisfy those needs using different types of antennas and other techniques [11] [12] [13].

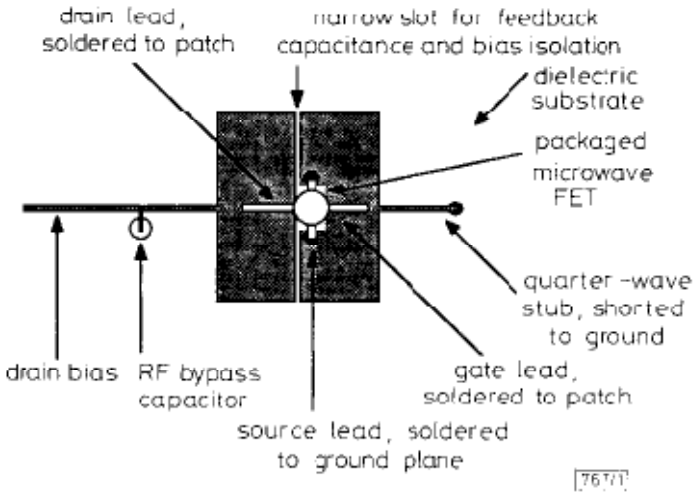

Figure 1.2: Illustration of the hybrid patch element with an integrated FET

Nowadays, One type of antenna structure that has been widely researched is the composite right/left-handed (CRLH) zeroth order resonance (ZOR) antenna. The ZOR antenna is realized by CRLH transmission lines (TLs) which can easily achieve unique metamaterial properties such as anti-parallel phase and group velocities, and a zero propagation constant [14] [15] [16] [17]. Especially, due to the zero propagation constant property in the left-handed (LH) metamaterial the ZOR antenna have an infinite wavelength and its resonant

frequency becomes independent to size of the resonator. Therefore, the ZOR antenna offers interesting features such as smaller size than conventional resonant antenna, and narrow bandwidth owing to high Q-factor of resonator [18] [19] [20]. More details about metamaterial and the ZOR antenna will be discussed in Chapter 2.

In this thesis, a power efficient active integrated antenna is proposed. The whole circuit is designed using the CPW technology. A CPW structure gives a lot of design freedom, it provides the benefits of easy design to implement the desired circuit parameters and makes it possible for monolithic integration. Moreover, the via free structure and single layer process results in a simpler fabrication process compared with micro-strip line technology structure. In order to occur the oscillation, the input impedance of active source part of the AIA, which contains FET and matching circuit, is designed to have negative impedance. The negative technology will be more discussed in chapter 3. For both load and radiating element, the CPW-fed ZOR antenna is employed [21]. Since the ZOR antenna has electrically small size, we can reduce the antenna size which is the most bulky part in conventional AIA design. Also, the high Q-factor of the electrically small size ZOR antenna helps to lower the phase noise of the AIA. In the oscillator design, the high harmonics are suppressed so that radiation loss of the AIA is decreased. As a result, we achieved 27.2% of DC to RF power conversion efficiency in the proposed AIA design. The proposed AIA has high DC to RF power conversion efficiency and compact size. Therefore, the proposed AIA can be a good candidate for spatial power combining application. The AIA design procedure will be discussed in chapter 3 and the methods of fabrication and measurement results will be demonstrated in chapter 4.

Chapter 2

Composite Right-/Left-Handed Metamaterials

2.1 Introduction

Recently, metamaterial have attracted a lot of attention in the engineering and scientific fields. Normally, Metamaterials are artificial materials engineered to have properties that may not be found in nature. However, much of the recent research has been focused on "metamaterials" that exhibit the unique property of simultaneous negative permittivity (ε) and permeability (μ) and are sometimes called "double negative materials" in theoretical research papers and articles. In this metamaterial, the group velocity and the phase velocity are in the opposite direction or anti-parallel, which means the E-field, H-field and phase velocity form a triad in left-handed fashion. Therefore, they are also refered as "left-handed materials". In addition, due to the negative ε and μ, the refractive index of the material is also negative, resulting in the term "negative refractive index material". They have extraordinary

electromagnetic properties that are rarely found in the natural materials. Therefore, they provide another concept and method for advancement of various type of microwave circuits and its applications. This kind of metamaterials were firstly proposed by Veselago [22] in 1967. he compared the properties of conventional substances characterized by positive permittivity and permeability, which can also be refered right-handed, or positive refractive with theoretical substances which can be considered negative permittivity and permeability. Pendry et al. used a periodic array of split ring resonators (SRR) to provide negative permeability [23]. A research team from University of California, San Diego (UCSD) combined the ring resonator and a metallic wire to develop a novel medium with simultaneously negative permeability and permittivity at microwave frequency [24]. Moreover, Smith et al. experimentally demonstrated the negative index of refraction that breaks the basic physic laws such as Doppler effect, Cherenkov radiation and Snell's law [25] [26]. However, those metamaterial which use the split ring resonator are lossy and it can only operate at resonant frequency. Thus, another methodology which employ transmission line approach is proposed by Itoh et al. and Eleftheriades et al. to realize the left-handed material [27] [28] [29].

2.2 Metamaterial Concept

When we consider the plane waves traveling in both positive and negative indexed (right-handed and left-handed) materials where $\vec{E} = \vec{E}_0 e^{-j\vec{k}\cdot\vec{r}}$ and $\vec{H} = \vec{H}_0 e^{-j\vec{k}\cdot\vec{r}}$, we can utilize Maxwell's equations to determine [30]

$$\vec{k} \times \vec{E} = \omega \vec{B} = \begin{cases} +\omega |\mu| \vec{H} & if \quad \mu > 0 \quad (RH) \\ -\omega |\mu| \vec{H} & if \quad \mu < 0 \quad (LH) \end{cases} \qquad (2.1)$$

$$\vec{k} \times \vec{H} = -\omega \vec{D} = \begin{cases} -\omega |\varepsilon| \vec{E} & if \quad \varepsilon > 0 \quad (RH) \\ +\omega |\varepsilon| \vec{E} & if \quad \varepsilon < 0 \quad (LH) \end{cases} \qquad (2.2)$$

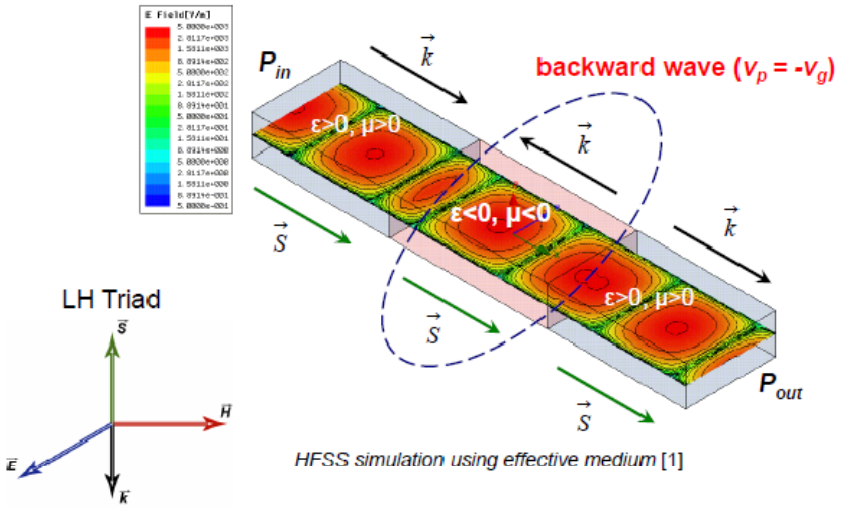

Figure 2.1: Left-handed(LH) triad and rectangular wave guide filled with LH Metamaterial

where the time dependence $e^{j\omega t}$ is assumed. In these equations $\vec{k}$ is the wave vector and indicates the direction that the plane of constant phase travels, or the orientation of the phase velocity (υ_s). When ε, μ> 0, these equations represent that the triad formed by $\vec{E}, \vec{H},$ and $\vec{k}$ will be right-handed, and when ε, μ < 0, the triad will be left-handed. Also, the Poynting vector, which can be expressed by $\vec{S} = \vec{E} \times \vec{H}^*$, will be right-handed in both types of materials. The Poynting vector indicates the power traveling direction, or the orientation of the group velocity (υ_g), so in a material with ε, μ > 0 the phase velocity (υ_p) and group velocity (υ_g) are parallel on the other hand, in a material with ε, μ < 0 the phase velocity (υ_p) and group velocity (υ_g) are anti-parallel. The Fig. 2.1 shows an illustration for LH metamaterial. As shown in the figure, if left-handed material is excited in rectangular wave

guide, then power will propagate away from the source, but that the plane of constant phase will propagate toward the source.

2.3 CRLH Transmission Lines

2.3.1 Distributed Models

One way to realize the metamaterial is using transmission line theory. As we will discuss later, these structures exhibit both effective positive ε and, μ and effective negative ε and, μ depending on the frequency, which results in the term "Composite Right/Left-Handed Transmission Lines" or simply "CRLH-TLs".

Theoretically, the propagation constant (γ) of a lossless TL can be defined as,

$$\gamma = j\beta = \sqrt{Z'Y'} \tag{2.3}$$

where Z' and Y' are per-unit length impedance and admittance, respectively. For the typical purely right-handed (PRH) transmission line, it consists of series inductance L_R and shunt capacitance C_R, as shown in Fig. 2.2(a).

By substituting $Z' = j\omega L_R$ and $Y' = j\omega C_R$, from Eq.(2.3) we can obtain

$$\beta_{PRH} = \omega\sqrt{L_R C_R} \tag{2.4}$$

As a result, we can obtain the dispersion diagram of PRH-TLs from Eq.(2.4) as shown in Fig. 2.2(b), which graphically represents the relationship between the phase constant β and the frequency ω.

In contrast, for the purely left-handed (PLH) transmission line, it consists of series capacitance C_L and shunt inductance L_L, as shown in Fig. 2.3(a). Once again using Eq.(2.3)

with $Z' = \frac{1}{j\omega C_L}$ and $Y' = \frac{1}{j\omega L_L}$, the propagation constants for the PLH transmission line can be respectively defined as

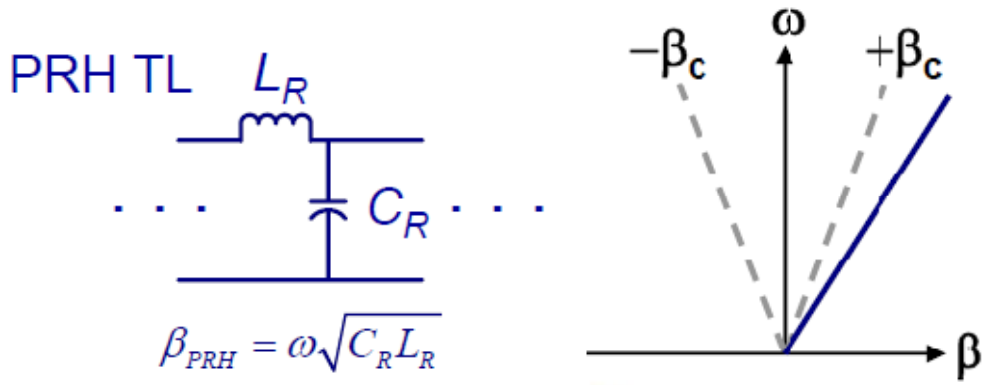

(a) (b)

Figure 2.2: Purely right-handed transmission line: (a) Circuit model for the unit cell and (b) Dispersion diagram for the unit cell.

$$\beta_{LH} = -\frac{1}{\omega\sqrt{L_R C_R}} \tag{2.5}$$

the dispersion diagram of PLH-TLs can be also obtained from the above equation as shown in Fig. 2.3(b).

From Fig. 2.2 and Fig. 2.3 , both group velocity ($\upsilon_g = \frac{\partial\omega}{\partial\beta}$) and phase velocity ($\upsilon_p = \frac{\omega}{\beta}$) can be observed in these dispersion diagrams. In Fig. 2.2(b), it can be found that υ_g and υ_p of a PRH-TL are parallel ($\upsilon_g \upsilon_p > 0$). From Fig. 2.3(b), υ_g and υ_p of a PLH-TL are anti-parallel ($\upsilon_g \upsilon_p < 0$). Furthermore, the dispersion curve shows υ_g tends towards infinity as

increases. Since this phenomenon violates Einstein's special theory of relativity, we can assume the PLH-TL does not exist, and therefore the RH parasitic effects are not avoidable.

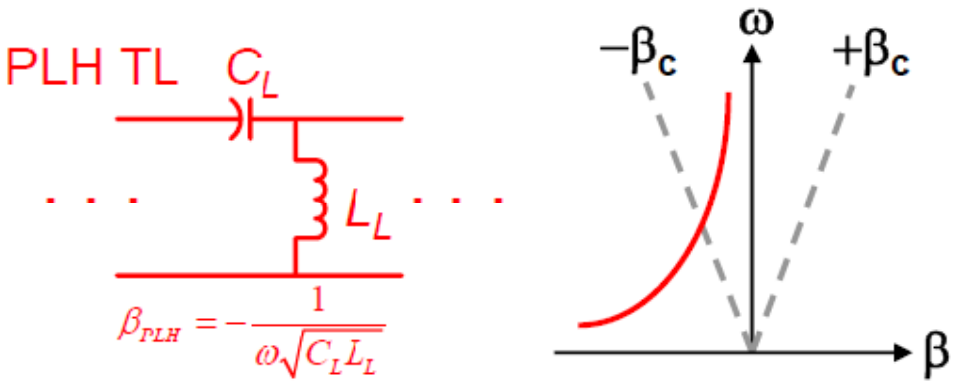

(a) **(b)**

Figure 2.3: Purely left-handed transmission line: (a) Circuit model for the unit cell and (b) Dispersion diagram for the unit cell.

In addition, for the PRH-TL, the propagation constant is proportional to the frequency and has positive value, which implies there is a phase delay along the purely right-handed transmission line. To the contrary, the PLH-TL propagation constant has negative value and it increases when the frequency decreases. Therefore, the phase velocity of the purely left-handed transmission line is negative, which indicates the phase advanced phenomena should be observed.

The structure that is purely LH for all frequencies is impossible to realize due to inevitable parasitic effects therefore, the Fig. 2.4(a) shows a more generalized circuit model which is a combination of both LH and RH transmission lines. The structure consists of both series and shunt inductances and capacitances and the unit cell size is d. By using the equation Eq.(2.3)

with $Z' = j\omega L_R + \frac{1}{j\omega C_L}$ and $Y' = j\omega C_R + \frac{1}{j\omega L_L}$ the dispersion relation of a CRLH TL can be calculated as

$$\beta_{CRLH} = s(\omega)\sqrt{\omega^2 L_R C_R + \frac{1}{\omega^2 L_L C_L} - \left(\frac{L_R}{L_L} + \frac{C_R}{C_L}\right)} \tag{2.6}$$

where

$$s(\omega) = \begin{cases} -1 & if\ \omega < \omega_2 = \min\left[\frac{1}{\sqrt{L_R C_L}}, \frac{1}{\sqrt{L_L C_R}}\right] \\ +1 & if\ \omega > \omega_1 = \max\left[\frac{1}{\sqrt{L_R C_L}}, \frac{1}{\sqrt{L_L C_R}}\right] \end{cases} \tag{2.7}$$

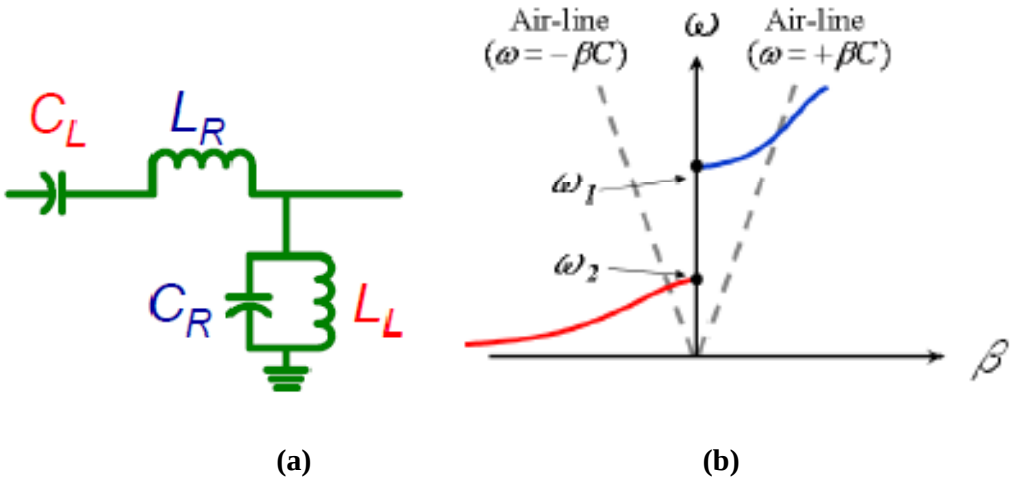

(a) **(b)**

Figure 2.4: Composite right/left-handed transmission line: (a) Circuit model for the unit cell and (b) Dispersion diagram for the unit cell.

The dispersion diagram for the CRLH-TL is shown in Fig. 2.4(b) and two different modes are observable. The upper mode has a positive group velocity and phase velocity and

represents RH in nature. The lower mode has a negative group velocity and phase velocity and represent LH in nature. Since the CRLH-TL has these two modes, the behavior of the structure depends on the operation frequency. Another things we can observe is that the dispersion curve, and thus the phase response of a CRLH-TL, is non-linear with respect to frequency.

2.3.2 Finite unit-cells Models

The previous section briefly explains the basic concept about an ideal CRLH-TL which does not exist in nature, especially for the LH range. However, a CRLH-TL can be realized using a periodical structure of electrically small lumped unit cell over a certain frequency range.

The infinitesimal length of equivalent circuit model for CRLH-TL is shown in Fig. 2.5. The TL can be realized by cascading N unit cell with period of d. The total length of the transmission line is N times d as shown in Fig. 2.6. Each unit cell in this periodic structure includes the series inductance (L_R), series capacitance (C_L), shunt capacitance (C_R) and shunt inductance (L_L) in this model.

By using the Bloch-Floquet periodic boundary condition and applying ABCD matrix of one unit cell, the eigenvalues can be calculated [31]:

$$\beta(\omega) = \frac{1}{p}\cos^{-1}\left(1+\frac{ZY}{2}\right) \tag{2.8}$$

where

$$Z(\omega) = j\left(\omega L_R - \frac{1}{\omega C_L}\right) \tag{2.9}$$

$$Y(\omega) = j\left(\omega C_R - \frac{1}{\omega L_L}\right)$$

The dispersion curve for the CRLH-TL can be characterized by four frequency points that occur at the boundary of the RH and LH mode, where β= -π/d, 0, and π/d.

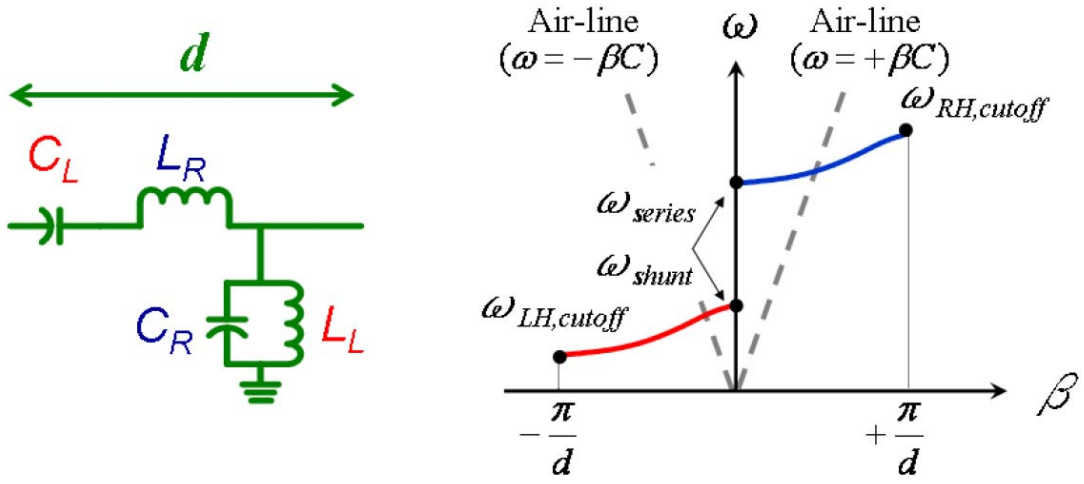

(a) **(b)**

Figure 2.5: The infinitesimal length of equivalent circuit model for CRLH-TL: (a) Circuit model for the unit cell of finite length d and (b) Dispersion diagram for the unit cell.

These points can be divided by the components in the equivalent circuit model as

$$\omega_{series} = \frac{1}{\sqrt{L_R C_L}} \tag{2.10}$$

$$\omega_{shunt} = \frac{1}{\sqrt{L_L C_R}} \tag{2.11}$$

$$\omega_{RH,cutoff} = \frac{2}{\sqrt{L_R C_R}} \tag{2.12}$$

$$\omega_{LH,cutoff} = \frac{1}{2\sqrt{L_L C_L}} \tag{2.13}$$

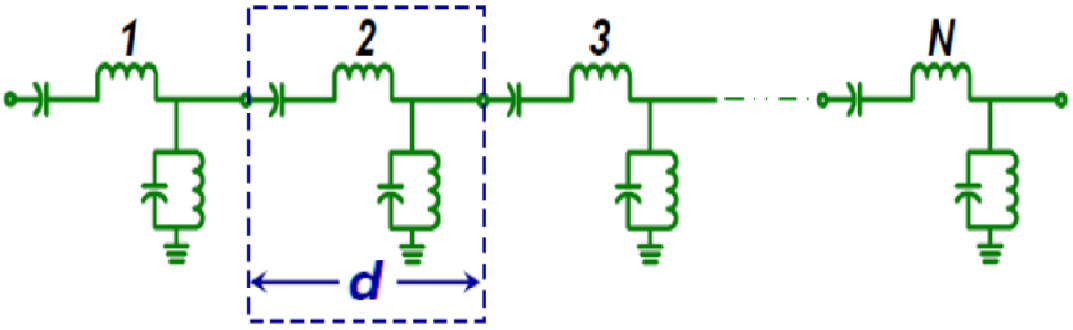

Figure 2.6: Cascade of n unit cell of composite right/left-handed transmission line.

The two frequencies at the point where β = 0 are ω_{shunt} which is the resonating frequency of the shunt elements in the circuit model and ω_{series} which is the resonating frequency of the series elements. A lower stop-band extends from DC to $\omega_{LH,cutoff}$, and an upper stop-band extends from $\omega_{RH,cutoff}$ to ∞. Moreover, a stop-band may take place between ω_{series} and ω_{shunt}, relying on the relationship between two impedances that are defined as

$$Z_R = \sqrt{\frac{L_R}{C_R}} \tag{2.14}$$

$$Z_L = \sqrt{\frac{L_L}{C_L}} \tag{2.15}$$

The relationship between these two LH and RH impedances decides the relationship between ω_{series} and ω_{shunt} and vice versa. For instance, if $Z_L < Z_R$, then $\omega_{series} < \omega_{shunt}$ and if $Z_L > Z_R$, then $\omega_{series} > \omega_{shunt}$. The zeroth order resonance (ZOR) can be expected within this stop band where $\beta = 0$. This ZOR will be discussed next section. On the other hand, under the certain condition that $Z_L = Z_R$, $\omega_{series} = \omega_{shunt}$ and structure is considered as a balanced CRLH-TL. The stop-band or spectral gap between the RH and LH mode do not exist for the balanced case.

2.4 Zeroth Order Resonance

In the impedance matched transmission line, when the wave propagates from input port to impedance matched port, it becomes a traveling wave. However, when the end of TL becomes short or open, the incident wave is all-reflected at the end of the TL and becomes a standing wave, then this TL ends up with being a resonator. Not only for RH TL case but also the CRLH TL can be a resonator when it becomes short or open at the end of TL. However, unlike with RH TL, the CRLH TL shows specific characteristics which is known as ZOR.

2.4.1 The principle of ZOR

In RH resonance case, the resonant frequencies are decided by physical length of resonator. The resonant condition can be expressed as,

$$l = m\frac{\lambda}{2} \quad \text{or} \quad \theta_m = \beta_m l = \frac{2\pi}{\lambda}\cdot\frac{m\lambda}{2} = m\pi \tag{2.16}$$

where $\beta_m l$ is electrical length of resonator and m is defined as m = +1, +2, +3, ...$+\infty$. Therefore, the periodic PRH TL has infinity resonant frequencies which can be expressed as $\omega_m = m\omega_1$ where the ω_1 is fundamental resonance frequency.

The Fig. 2.7 illustrates the homogeneous balanced mode CRLH TL dispersion diagram and field distribution. Unlike PRH RL the CRLH TL can possess β=0 or negative integer, thus the electrical length ($\theta = \beta l$) can also be 0 or negative value. This can be defined as,

$$l = |m|\frac{\lambda}{2} \quad \text{or} \quad \theta_m = \beta_m l = \frac{2\pi}{\lambda} \cdot \frac{m\lambda}{2} = m\pi \tag{2.17}$$

and m can be defined as

$$m=0, \pm1, \pm2, \pm3, ..., \pm\infty \tag{2.18}$$

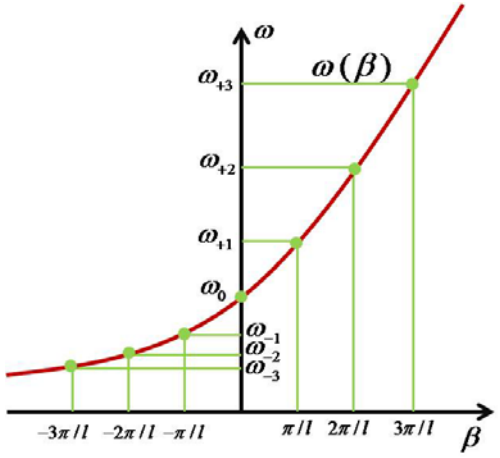

(a)

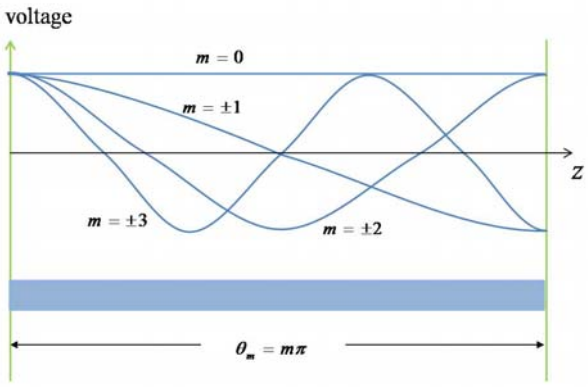

(b)

Figure 2.7: The balanced mode CRLH TL (a) the relationship between resonant frequency and phase constant. (b) the field distribution of resonance

Therefore, there are some observations for the specific characteristic of the CRLH TL comparing with RH TL. first, there are not only positive (m > 0) resonance frequencies but also, negative (m < 0) resonance frequencies in the CRLH TL. Second, as it is illustrated in Fig. 2.7(b), when the absolute value of resonance frequency is the same (that is, -m, +m), the field distribution of the resonance is the same except m=0 case. third, Since the nonlinearity feature of dispersion diagram of CRLH TL, the resonant frequencies is not linear. Especially, there is more nonlinearity curve in the LH region, the negative resonant frequencies are concentrated on lower frequency region as shown in Fig. 2.7(a). Last, the resonant mode for m=0 is specifically called zeroth order resonance and it shows a flat field distribution characteristic. Therefore, the CRLH TL shows resonant feature in this ZOR mode regardless of physical length of the resonance.

2.4.2 The ZOR basic characteristics

The resonance is available when the TL is shorted or opened at the end so that there are only standing waves in the TL. For the open-ended case the input impedance $Z_{in-open}$ can be shorten as

$$Z_{in-open} = -jZ_c \cot(\beta l)|_{\beta \to 0} \approx -jZ_c \frac{1}{\beta l}$$

$$= -j\sqrt{\frac{Z'}{Y'}}\left(\frac{1}{-j\sqrt{Z'Y'}}\right)\frac{1}{l} = \frac{1}{Y'l} = \frac{1}{Y'(Np)} = \frac{1}{NY} \qquad (2.19)$$

The Y is an admittance of unit cell which can be defined as $Y = j[\omega C_R - 1/(\omega L_L)]$. Since the N is just integer number, the resonant frequency of total resonance is the same as resonant frequency of admittance Y. Therefore, there is only one resonant frequency which can be defined as

$$\omega_{r\cdot open} = \omega_{sh} = \frac{1}{\sqrt{L_L C_R}} \tag{2.20}$$

On the other hand, the short-ended input impedance can be shorten as

$$Z_{in-short} = -jZ_c \tan(\beta l)|_{\beta \to 0} \approx -jZ_c \beta l$$

$$= -j\sqrt{\frac{Z'}{Y'}}\left(-j\sqrt{Z'Y'}\right)l = Z'l = Z'(Np) = NZ \tag{2.21}$$

The Z is an impedance of unit cell which can be defined as $Z = j[\omega L_R - 1/(\omega C_L)]$. Since the N is also integer number, the resonant frequency of total resonance is the same as resonant frequency of impedance Z. Therefore, there is only one resonant frequency which can be defined as

$$\omega_{r\cdot short} = \omega_{se} = \frac{1}{\sqrt{L_R C_L}} \tag{2.22}$$

An important observations are that there is no ω_{se} resonance at the open-ended TL case, and also there is no ω_{sh} resonance at the short-ended TL case. However, for the balanced mode case, the resonant frequency ω_{sh} and ω_{se} is the same and both short-ended and open-ended TL have the same ZOR frequency.

Another interesting ZOR feature is that resonance frequency is only depends on the L_L / C_R or L_R / C_L of unit-cell CRLH TL regardless of physical length of resonance. Therefore, the ZOR can be implemented within the size where enough inductance and

capacitance value is realized. This specific feature make it possible to design an electrically small ZOR antenna.

The unloaded Q-factor of ZOR shows a different feature with conventional RH resonator due to the infinitive wavelength. First of all, in the open-ended case, the impedance of L_L and C_R is proportional to 1/N. Therefore the impedance L, C, and G is expressed as L_L/N, $N \cdot C_R$, and $1/(N \cdot G)$ where the G represents conductance which indicates parasitic resistance of inductance or leakage current of capacitance. The equivalent circuit model is illustrated in Fig. 2.8.

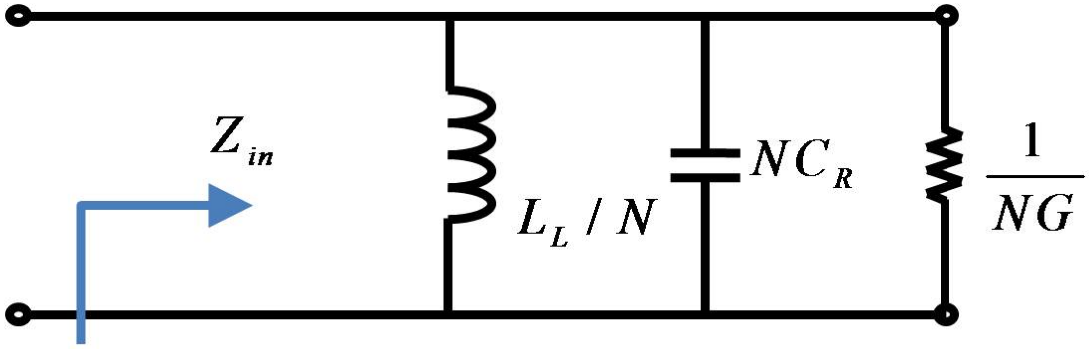

(a)

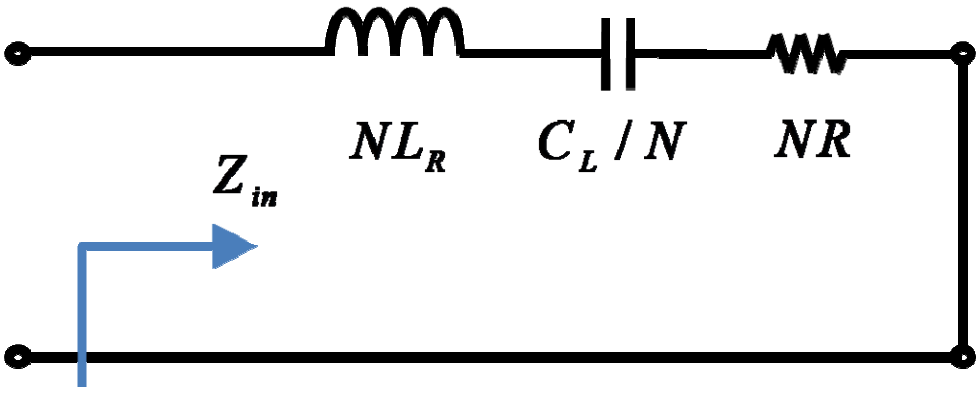

(b)

Figure 2.8: Input immitance of CRLH TL resonator (a) open-ended (b) short-ended.

The unloaded Q-factor of ZOR in open-ended case can be calculated as

$$Q_{u-open} = \frac{1/NG}{\omega_{sh}(1/NG)} = \frac{1/G}{\omega_{sh}L_L}$$

$$= \omega_{sh}(1/NG)\cdot(NC_R) = \omega_{sh}(1/G)\cdot(C_R)$$

$$= \frac{1}{G}\sqrt{\frac{C_R}{L_L}} \tag{2.23}$$

In this case, the loss only comes from conductance G regardless of series loss R. The series loss R is the model of parasitic resistance of series inductance or leakage resistance of series capacitance which is connected with L_R and C_L in series. In the open-ended case, since the field distribution is flat, there is no voltage difference between nodes. This results in no current flows through R and no loss generated in R. Therefore, the loss in this case is only generated by conductance G.

On the other hand, the admittance L, C, and G of short-ended case can be expressed as $N\cdot L_R$, C_L/N, and $N\cdot R$. Also, the unloaded Q-factor can be calculated as

$$Q_{u-short} = \omega_{se}\frac{NL_R}{NR} = \frac{\omega_{se}L_R}{R}$$

$$= \frac{1}{\omega_{se}NR\cdot C_L/N} = \frac{1}{\omega_{se}R\cdot C_L}$$

$$= \frac{1}{R}\sqrt{\frac{L_R}{C_L}} \tag{2.24}$$

Similarly, in the short-ended case unloaded Q-factor loss is only existed on R. Since the field distribution is flat, the current does not flow through G.

2.4.3 The ZOR radiation characteristic

Generally, the CRLH TL radiation characteristic is based on leaky wave. While incident wave travels through the TL structure, the traveling wave leaks the wave power to outside of structure to radiate waves. However, when the CRLH TL becomes open-ended or short-ended, the standing wave is generated and due to the resonance characteristic the wave radiation is formed. Especially, Since ZOR have constant field distribution along the CRLH structure, the wave radiates toward broadside.

A specific resonant characteristic of ZOR is that the ZOR have infinitive wavelength. Also, since it has a constant field distribution, resonance frequency of ZOR only depends on reactance of unit cell regardless of its physical length. This ZOR feature has a lot of potential advantages for antenna application. One of the advantages is size reduction. Generally, in electrically small antenna case, the current distribution is concentrated on a small region due to the small size, therefore loss is increased in the antenna. However, the ZOR antenna has a constant field distribution and because of the constant field distribution, the current is not concentrated on a small region and results in reduced loss. Therefore, the radiation efficiency of ZOR is increased. Moreover, electrically small antenna has lower gain and directivity. However, we can increases the gain and directivity of ZOR antenna with many unit cell of ZOR.

2.5 A CPW-fed ZOR Antenna

A compact CPW-fed ZOR antenna is introduced in this section [21]. The antenna is modeled on a CPW single layer where vias are not needed. As it is explained previous section, the antenna size reduction is realized by ZOR phenomenon. The CRLH unit cell on a vialess single layer simplifies the fabrication process and design freedom. By taking advantage of the design freedom, bandwidth extension technique is proposed on the antenna design. As a result, three different ZOR antenna design is proposed. Each antenna have different characteristics that are size reduction, higher efficiency, easier manufacturing, and extended bandwidth. In this thesis, only a chip-loaded ZOR will be discussed and employed for use of AIA.

The chip loaded ZOR antenna are shown in Fig. 2.9. The proposed chip-loaded antenna is designed based on a CRLH TL. The antenna consists of two unit cells that each unit-cell has a metallic patch and two mounted chip inductors on both sides. The metallic patch size on center is decided to have less than fundamental frequency wavelength to satisfy a homogeneous condition and thus achieve a zero phase constant. In this antenna configuration the gaps between metallic patches acts as a series capacitance C_L. A shunt capacitance C_R is decided by the gap between the metallic patches on the top and another metallic patch on the bottom side of the substrate. Also, the gap between metallic patch on the top of the substrate and CPW ground affects the shunt capacitance C_R. The metallic patch represents a series inductance L_R. The shunt inductance L_L is increased by employing the chip inductor between the patch and CPW ground. Since the proposed antenna has an open-ended termination, the ZOR frequency can be decided by shunt capacitance and inductance as it is discussed in previous section. Since the antenna can have a high shunt inductance due to the chip inductor, this antenna is applicable for low frequency applications. The chip-inductor ZOR antenna is realized with high frequency chip inductance of 8.2nH. Therefore, this antenna has a ZOR frequency at 2.32GHz. The antenna is also fabricated on a Rogers RT/Duroid 5880 substrate

with a permittivity of 2.2 and thickness of 1.6 mm. The size of the antenna is 18mm×23mm ($0.13\lambda_o \times 0.17\lambda_o$).

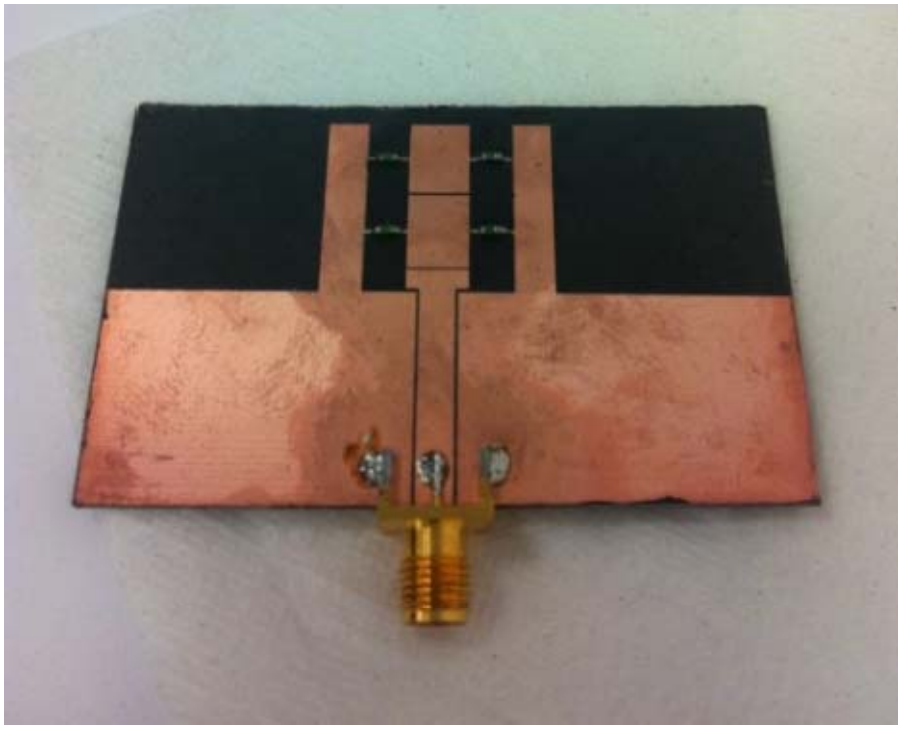

Figure 2.9: A Prototype of Chip-Loaded ZOR Antenna

The measured reflection coefficient are shown in Fig. 2.10. The reflection coefficients is lower than -10dB near the ZOR frequency 2.32GHz with bandwidth of 8.9%. The Fig. 2. 11 shows the measured radiation patterns on the E-plane (90º) and H-plane (0 º) at 2.32GHz. The cross-polarization is 8dB lower than co-polarization in E-plane and 20dB lower in H-plane. The antenna has a gain of 1.54dBi at the ZOR frequency.

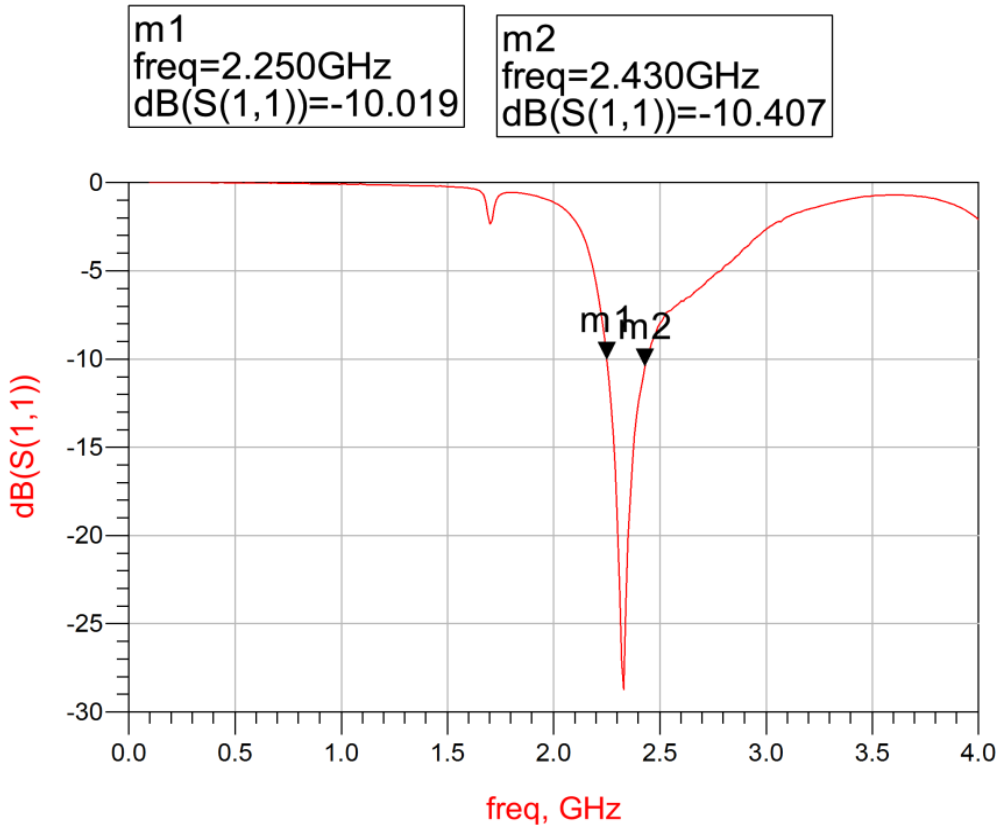

Figure 2.10: The measured reflection coefficient of the chip loaded ZOR antenna.

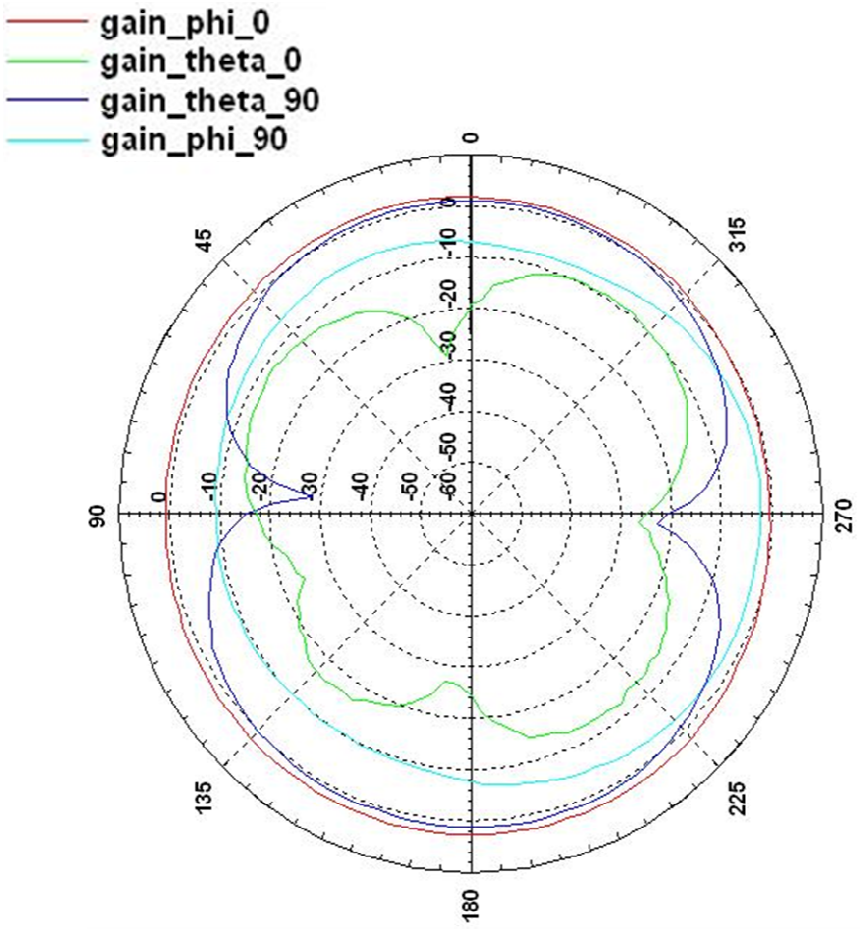

Figure 2.11: The measured radiation pattern of the chip loaded ZOR antenna at 2.32GHz.

Since the antenna is designed using CPW technology, it serves a lot of design freedom for AIA design. Also, the antenna has electrically small size and high Q-factor. Therefore, this ZOR antenna can be a good candidate for AIA design application and array system. This chip loaded ZOR antenna will be utilized for AIA design in next chapter.

Chapter 3

Oscillator Design for Active Integrated Antenna

3.1 Introduction

Active integrated antenna (AIA) is divided by source and radiating part. The source part generates the oscillating signal and it is consisted of active device such as FET and radiating part is consisted of antenna, In this chapter, we will discuss about how to design the active part of AIA. At first, the condition of oscillators and negative-resistance oscillation method for design of AIA is discussed. Then, overall procedure of the proposed AIA will be demonstrated through this chapter.

3.2 Theory of Oscillators

Generally, an oscillator is a nonlinear circuit which has function of converting DC powers to an AC waveform. Most RF oscillators serve sinusoidal outputs, which minimizes unwanted harmonics and noise sidebands. The basic operational concept of a sinusoidal

oscillator can be described with the linear feedback approached circuit shown in Fig. 3.1. In the figure 3.1, An amplifier with voltage gain A has an output voltage V_0. This voltage passes through a feedback network with a frequency dependent transfer function *H(ω)*, and is added to the input V_i of the circuit. Thus the output voltage can be expressed as

$$V_0(\omega) = AV_i(\omega) + H(\omega)AV_0(\omega), \tag{3.1}$$

which can be solved to result in the output voltage in terms of the V_i as

$$V_0(\omega) = \frac{A}{1 - AH(\omega)} V_i(\omega) \tag{3.2}$$

When the denominator of Eq. (3.2) becomes zero at a particular frequency, it becomes possible to obtain a non-zero output voltage for a zero input voltage, thus generating oscillation. This is known as the Nyquist criterion. In contrast to the design of an amplifier, where maximum stability is required, oscillator design is based on an unstable circuit [32].

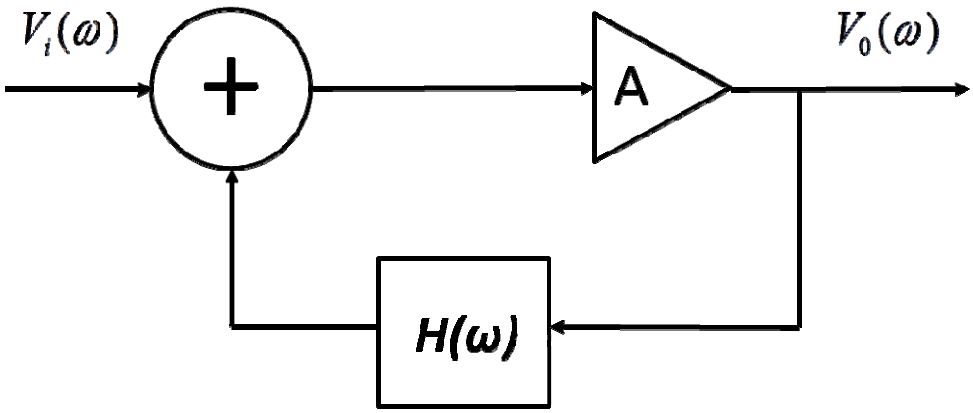

Figure 3.1: Block diagram of a sinusoidal oscillator using an amplifier with feedback path

3.3 Negative-Resistance Oscillator

3.3.1 Negative-resistance method

Another design approach for microwave frequency oscillators is the negative resistance method. If an amount of energy is supplied equal to the energy dissipated in a circuit, the circuit can sustain oscillations. The behavior of the active device can be expressed by a negative resistance in series with a reactance, as shown in Figure 3.2. The negative-resistance device is expressed by the amplitude and frequency dependent impedance as

$$Z_{IN}(A, \omega) = R_{IN}(A, \omega) + jX_{IN}(A, \omega) \tag{3.3}$$

Where A is the amplitude of i(t) and $R_{IN}(A, \omega) < 0$.

The oscillator is built by combining the device to a passive impedance denoted by

$$Z_L(\omega) = R_L(\omega) + jX_L(\omega) \tag{3.4}$$

if $R_L(\omega) + R_{IN}(A, \omega) > 0$, the total loop resistance in Figure 3.2 is positive and the oscillation will cease. The oscillation will be generated at the frequency (ω_o) and amplitude (A_o) where

$$Z_{IN}(Ao\ ,\ \omega_o) + Z_L(\omega_o) = 0 \tag{3.5}$$

Substituting (3.3) and (3.4) into (3.5), the important oscillation conditions can be represented as

$$R_{IN}(Ao\ ,\ \omega_o) + R_L(\omega_o) = 0 \tag{3.6a}$$

and

$$X_{IN}(Ao\ ,\ \omega_o) + X_L(\omega_o) = 0 \tag{3.6b}$$

Since the load is passive, $R_L > 0$ and thus, Eq. 3.6a indicates that $R_{in} < 0$. Therefore, While a positive resistance indicates energy dissipation, a negative resistance indicates an energy source. The frequency of oscillation can be controlled condition of Eq. 3.6b. The condition in (3.5), that $Z_L=-Z_{in}$ for steady-state oscillation, indicates that the reflection coefficients Γ_L and Γ_{in} are related as,

$$\Gamma_L = \frac{Z_L - Z_0}{Z_L + Z_0} = \frac{-Z_{in} - Z_0}{-Z_{in} + Z_0} = \frac{Z_{in} + Z_0}{Z_{in} - Z_0} = \frac{1}{\Gamma_{in}} \tag{3.7}$$

If

$$R_L(\omega) + R_{IN}(A, \omega) < 0 \tag{3.8}$$

the oscillation becomes unstable and its amplitude will increase. From (3.8), we know that the circuit in Figure 3.2 becomes unstable if the net loop resistance is negative; that is, when

$$|R_{IN}(A, \omega)| > R_L(\omega) \tag{3.9}$$

The start oscillation condition (3.9) is required in a well-designed oscillator. That is, when the amplitude A is small the oscillations will be generated. The start of oscillation condition in (3.9) is typically represented in the form of

$$|R_{IN}(0, \omega)| > R_L(\omega) \tag{3.10}$$

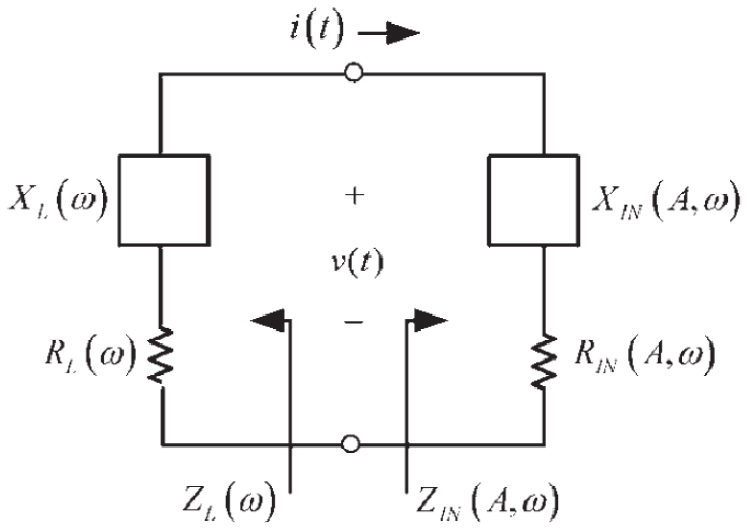

Figure 3.2: A negative-resistance model.

The oscillations will be generated as long as the loop resistance is negative. The amplitude of the current becomes a steady state value with the zero loop resistance and the condition of (3.6a) and (3.6b). In order to meet the start of oscillation condition in (3.10), the build-up of oscillations in (3.9), and the oscillation conditions in (3.6a) and (3.6b), the impedance Z_{IN} (A,ω) should be amplitude and frequency dependent. A conventional negative-resistance variation generated by the active device is such that at the beginning of oscillations $R_{IN}(0,\omega)$ has its maximum value and then, as the amplitude increases, $R_{IN}(0,\omega)$ decreases linearly. When R_{IN} reaches the value $R_{IN}(A_o, \omega)$, the condition of (3.6a) and (3.6b) are approximately satisfied in the circuit and the circuit will generate the oscillation with amplitude A_o at ω_o. Since $Z_{IN}(A, \omega)$ is amplitude and frequency dependent, the oscillation frequency decided by the condition of (3.6a) and (3.6b) might not be stable. Therefore, it is required to find another condition which can makes sure a stable oscillation. If the variation of $Z_{IN}(A, \omega)$ can be neglected for small variations around ω_o, Kurokawa [33] has shown that a stable oscillation is achieved when (3.6a) and (3.6b) are satisfied, and the condition below is also satisfied:

$$\left.\frac{\partial R_{IN}(A)}{\partial A}\right|_{A=A_o} \left.\frac{\partial X_L(\omega)}{\partial \omega}\right|_{\omega=\omega_o} - \left.\frac{\partial X_{IN}(A)}{\partial A}\right|_{A=A_o} \left.\frac{\partial R_L(\omega)}{\partial \omega}\right|_{\omega=\omega_o} > 0 \qquad (3.11)$$

The derivation of (3.11) is given in [34].

In many cases

$$\frac{dR_L(\omega)}{d\omega} = 0$$

(i.e., R_L is a constant) and (3.11) simplifies accordingly. Also, when R_L shows constant value the term $R_L(\omega_o)$ in (3.8) can be changed to the constant value R_L.

It is approximately assumed that $R_{IN}(A, \omega)$ and $X_{IN}(A, \omega)$ are only a function of the amplitude of i(t) for frequencies around the oscillation frequency. That means, in some cases the variation for $R_{IN}(A, \omega)$ can be approximately defined by

$$R_{IN}(A,\omega) \approx R_{IN}(A) = -R_o(1-\frac{A}{A_M}) \qquad (3.12)$$

where $-R_0$ represents the value of $R_{IN}(A)$ at A = 0, and A_M represents the maximum value of A. Putting it differently, the magnitude of the negative resistance shows a linearly decreasing function of A (see Figure 3.3).

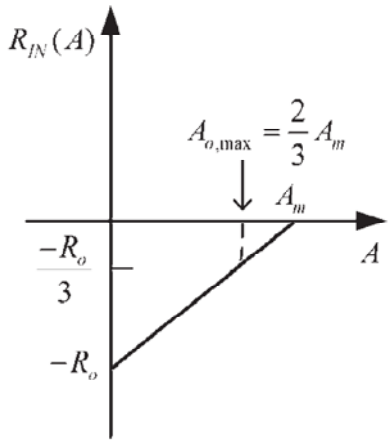

Figure 3.3: Linear variation of the negative resistance as a function of the current amplitude.

Practically, the value of R_L is selected for maximum oscillator power. In Figure 3.2, if R_{IN} is given by (3.12), the power delivered to R_L by R_{IN} is

$$P = \frac{1}{2}\mathrm{Re}(VI^*) = \frac{1}{2}|I|^2 |R_{IN}(A)| = \frac{1}{2}A^2 R_o(1-\frac{A}{A_M})$$

Hence, the value of A that occurs maximum oscillation power is decided from

$$\frac{dP}{dA} = \frac{1}{2}R_o(2A - \frac{3A^2}{A_M}) = 0$$

which provides the desired value of A, represented by $A_{o,max}$, that maximizes the power. That is,

$$A_{o,\max} = \frac{2}{3}A_M$$

At $A_{o,max}$ the value of $R_{IN}(A_{o,max})$ is

$$R_{IN}(A_{o,\max}) = -\frac{R_o}{3}$$

Hence, a appropriate value of R_L, which makes the maximum oscillator power, can be

$$R_L = \frac{R_o}{3} \tag{3.13}$$

Observe that (3.13) is possible when the negative input resistance varies linearly with amplitude. In practice, the selection of R_L, according to (3.13), shows good results.

3.3.2 Two-port negative-resistance oscillators

Figure 3.4 illustrate that a two port network is connected with a source E_s and source impedance Z_s on the left side and a load Z_L on the right side. Its S-parameter, which measured

in a Z_o system, helps to characterize the two port network. The input and output reflection coefficients are shown as

$$\Gamma_{IN} = S_{11} + \frac{S_{12}S_{21}\Gamma_L}{1 - S_{22}\Gamma_L} = \frac{S_{11} - \Delta\Gamma_L}{1 - S_{22}\Gamma_L} \tag{3.14}$$

and

$$\Gamma_{OUT} = S_{22} + \frac{S_{12}S_{21}\Gamma_s}{1 - S_{11}\Gamma_s} = \frac{S_{22} - \Delta\Gamma_s}{1 - S_{11}\Gamma_s} \tag{3.15}$$

where

$$\Delta = S_{11}S_{22} - S_{21}S_{12}$$

$$\Gamma_s = \frac{Z_s - Z_o}{Z_s + Z_o}$$

and

$$\Gamma_L = \frac{Z_L - Z_o}{Z_L + Z_o}$$

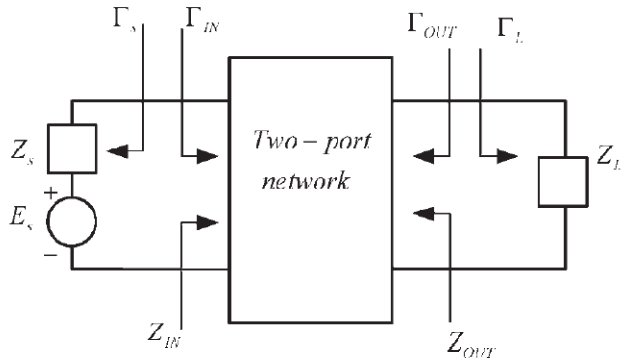

Figure 3.4: A two-port network connected to a source and a load.

The Figure 3.5 (a, b) shows general block diagrams for two-ports negative-resistance oscillators. Its S parameters help to characterize the transistor network, Z_T represents the terminating network impedance, and Z_L represents the load impedance. The notation used in Figure 3.5 (a, b) shows that in an oscillator the ports either side of the transistor can be used as the terminating port. One of the terminating ports is selected, the other port can be the input port. The load-matching network should be connected to the input port, showing agreement with the one port notation.

When the two-port is possibly unstable, an appropriate Z_T allows the two port to be represented as a one-port negative-resistance device which has a input impedance Z_{IN}, as shown in Figure 3.2.

When the input port is built to oscillate, the terminating port also generates oscillation. This oscillating phenomenon on both side ports can be proven as follows. The input port is oscillating when

$$\Gamma_{IN}\Gamma_L = 1 \tag{3.16}$$

and from (3.14) and (3.16), it follows that (after replacing Γ_L with Γ_T)

$$\Gamma_L = \frac{1}{\Gamma_{IN}} = \frac{1 - S_{22}\Gamma_T}{S_{11} - \Delta\Gamma_T}$$

or

$$\Gamma_T = \frac{1 - S_{11}\Gamma_L}{S_{22} - \Delta\Gamma_L} \tag{3.17}$$

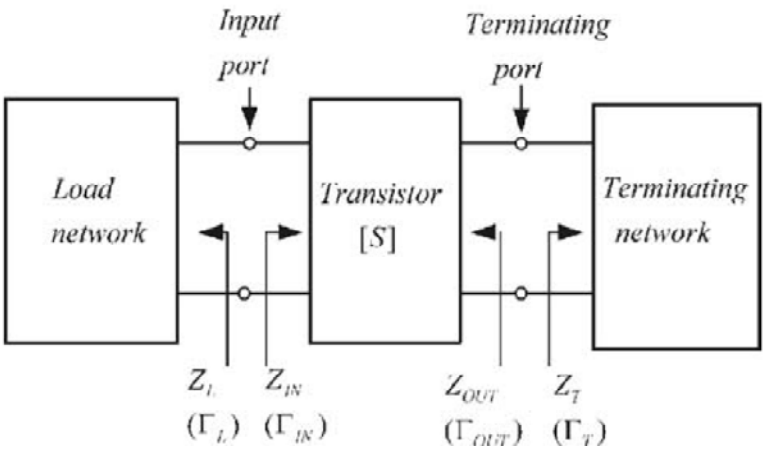

(a)

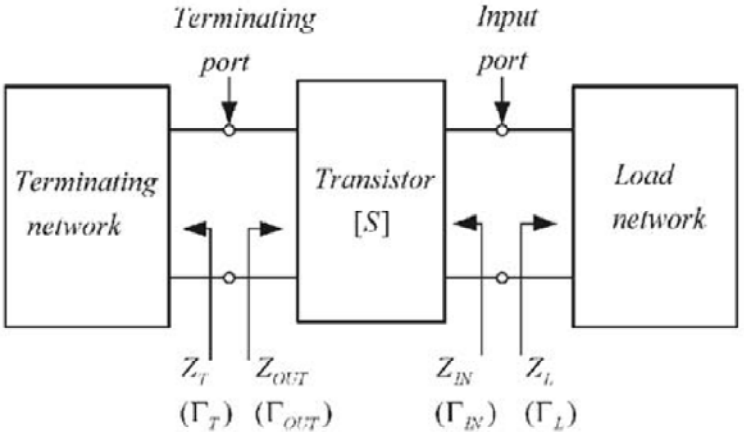

(b)

Figure 3.5: (a) Two-port oscillator models and (b) alternate representation.

Also, from (3.15)

$$\Gamma_{OUT} = \frac{S_{22} - \Delta\Gamma_T}{1 - S_{11}\Gamma_T} \tag{3.18}$$

Hence, from (3.17) and (3.18) it shows that

$$\Gamma_{OUT}\Gamma_L = 1$$

which indicates that the terminating port is also oscillating.

Based on the small-signal S parameters, a two port oscillator basic design procedure can be as follows [34]:

1. Use a potentially unstable transistor at the desired frequency of oscillation ω_o .
2. Design the terminating network to make $|\Gamma_{IN}| > 1$. Series or shunt feedback can be used to increase $|\Gamma_{IN}|$.
3. Design the load network to resonate Z_{IN}, and to satisfy the start of oscillation condition in (3.10). That is, let

$$X_L(\omega_o) = -X_{IN}(\omega_o) \tag{3.19}$$

and

$$R_L = \frac{|R_{IN}(0,\omega)|}{3} \tag{3.20}$$

This design procedure shows high rate of success for generating the oscillation. However, Since the whole design procedure is based on the small-signal S parameters, it cannot be used to exactly characterize the oscillator performance. This is because the oscillation power increases until the absolute values of negative resistance is equal to the load resistance and X_{IN} varies as a function of A which represents oscillation power. Therefore, the frequency of oscillation will shift somewhat from its designed value at ω_o. In this design procedure the oscillator power cannot be predicted. Also, the harmonics cannot be calculated.

3.4 Oscillator Design for AIA

In this section, the AIA design procedure is demonstrated using Advanced Design System (ADS) tools. Especially, the procedure of designing a power efficient AIA using ZOR antenna is introduced in details.

3.4.1 Co-planar waveguide technology

In this thesis, the whole circuit is designed using the co-planar waveguide (CPW) technology. A CPW transmission line (TL) is a structure that consists of a strip of thin metallic film deposited on the surface of a dielectric substrate with two ground electrodes running adjacent and parallel to the strip on the same surface [35]. A CPW structure provides a lot of design freedom, it gives the benefits of easy design to implement the desired circuit parameters and makes it possible for monolithic integration. Also, since the CPW structure has no via, a single layer CPW process results in a simpler fabrication process compared with micro-strip line technology structure.

3.4.2 A power efficient AIA using ZOR antenna

The basic idea of designing a power efficient AIA is that since the ZOR antenna resonant frequencies are not periodic due to the nonlinearity of CRLH TL property, the oscillating harmonic frequencies from oscillator can be adjusted to be away from the antenna higher order mode frequencies. Therefore, we can design the AIA that almost only radiates the wave at fundamental operating frequency by suppressing waves at the other higher harmonic oscillating frequencies. By doing so, we can reduce radiation loss of higher order mode in the AIA. As a result, the DC-RF conversion power efficiency of the AIA can be increased.

The figure 3.6 shows the schematic of the power efficient AIA circuit. The simulation is performed using ADS. In order to design oscillator three terminal device is used and therefore, two port negative resistance oscillator is designed. The CPW-fed ZOR antenna which is introduced in Chapter 2 is used for its load network. To generate oscillation the impedance transformed from the measured S-parameter of the passive ZOR antenna is applied for this load network in this simulation.

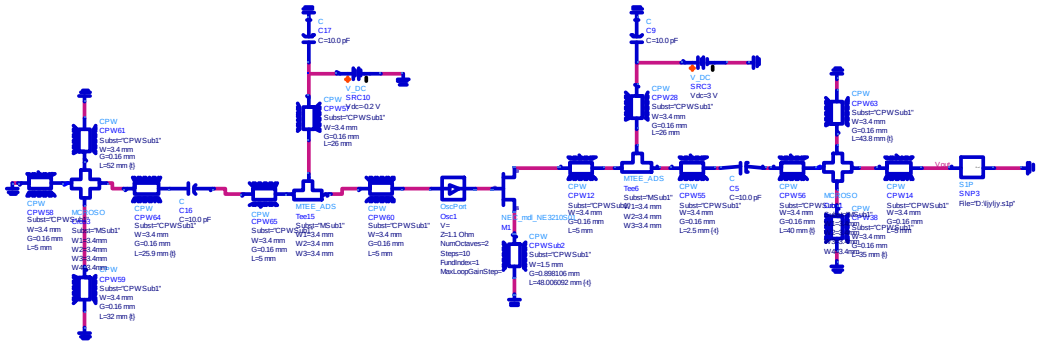

Figure 3.6: The schematic of the proposed AIA circuit.

The oscillation result of the proposed AIA design is shown in Fig. 3.7. It shows that the first harmonic oscillating frequency has 11.122dBm power at 2.34GHz, second harmonic frequency has -13dBm power at 4.679GHz, third harmonic frequency has 0.357dBm power at 7.019GHz, forth harmonic frequency has 0.357dBm power at 7.019GHz, and the other higher harmonic power is extremely small comparing with first harmonic.

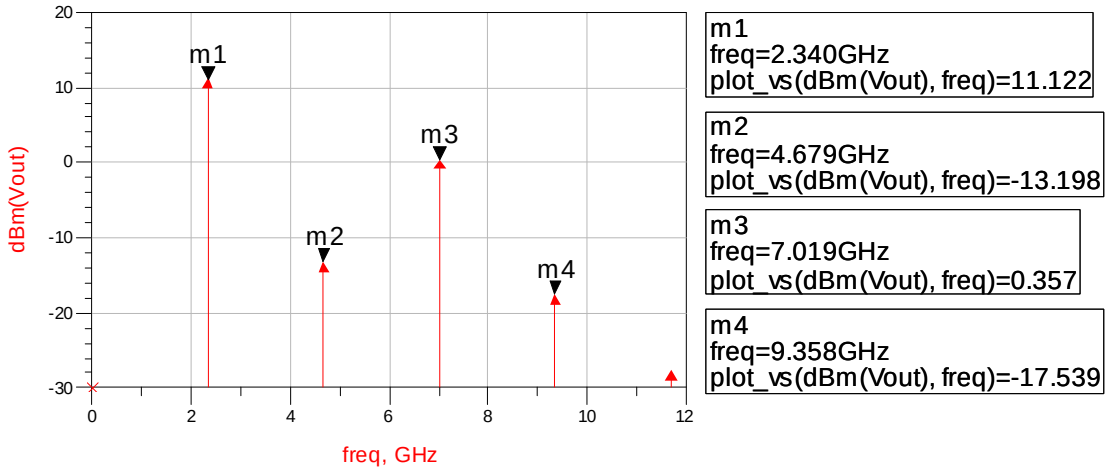

Figure 3.7: Oscillator results with oscillating harmonic frequencies and power.

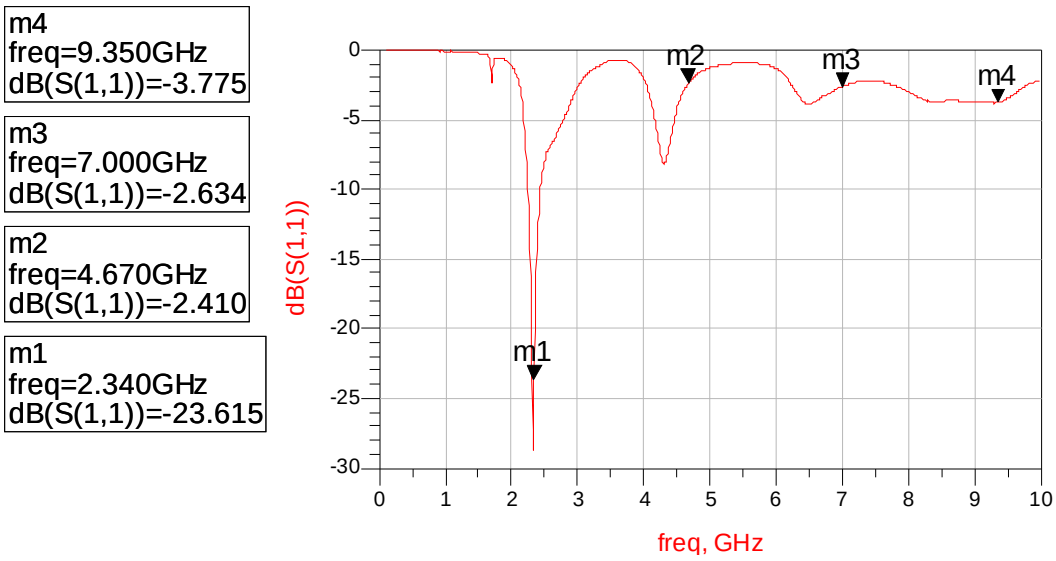

Figure 3.8: The return loss (S11) of the passive ZOR antenna (markers indicate the oscillating harmonics from oscillator)

The figure 3.8 shows the return loss of the passive ZOR antenna. As it is indicated in the Fig. 3.8, the high order harmonic frequencies is not matched with higher mode frequencies of the passive ZOR antenna. From the simulation result, this AIA design is assumed to have reduced radiation loss and therefore, high DC-RF conversion efficiency. The verification of this simulation will be discussed next chapter.

Chapter 4

Prototype and Measurement

4.1 Prototype

The Figure 4.1 shows a prototype of power efficient oscillator type AIA. The proposed power efficient AIA is fabricated on a 1.6mm Rogers RT/Duroid 5880 substrate which has 2.2 dielectric constant. The fabrication is conducted by lithography technology. A NEC super noise pseudomorphic Hetero-junction Field Effect Transistor(HJFET), model NE3210S01, is used for active device. The AIA is biased with V_{DS}=3V and V_{GS}=-0.2V at the end of quarter wavelength transmission line (TL). The quarter wavelength TL is designed to prevent the RF signal from flowing to the ground. As it is shown in the Fig 4.1, the source terminal of transistor is connected with TL, which plays a role of source inductance, in order to make the circuit more unstable. The 10pF capacitors mounted on the circuit used to short the RF signal and block the DC current. Therefore, the RF signal becomes shorted at the end of the quarter wave stub and the DC bias current is open to the ground. The short stubs on both side of the transistor and series CPW-TL are employed for matching circuits. In this AIA design, the chip inductor-loaded ZOR antenna is used and its size is 18mm×23mm ($0.13\lambda_o \times 0.17\lambda_o$).

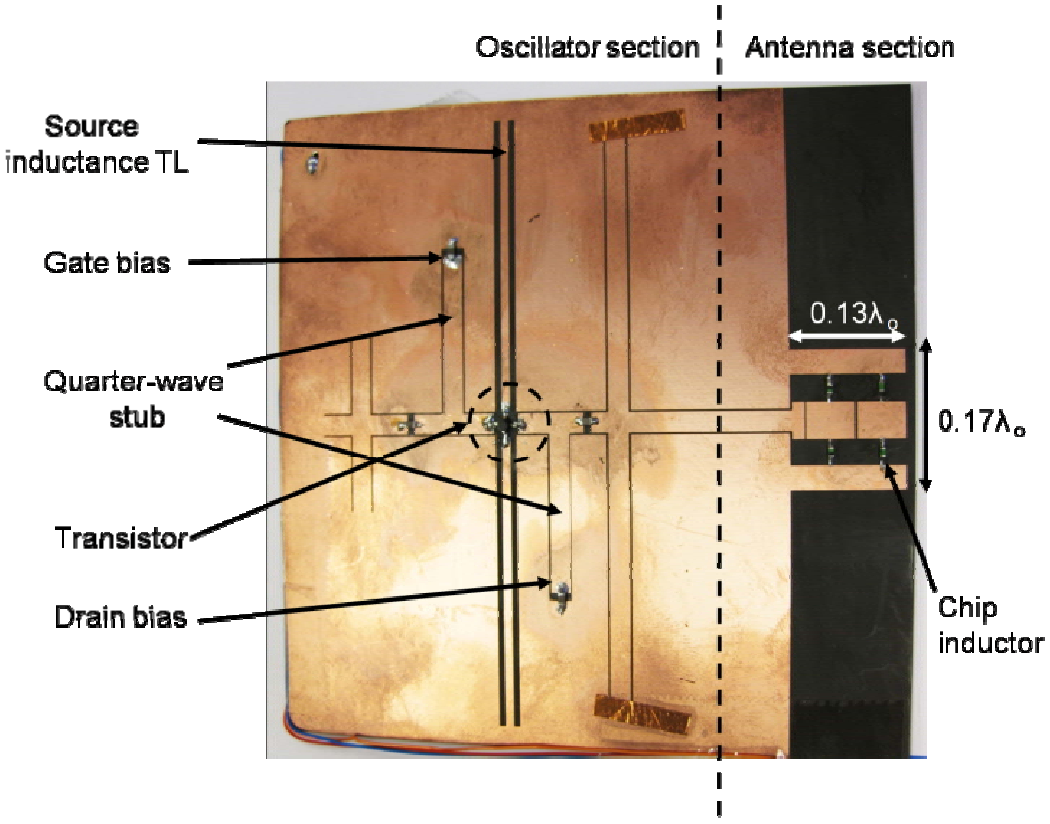

Figure 4.1: A prototype of the power efficient oscillator type AIA

4.2 Measurement and Performance

The measurement of AIA radiation pattern is conducted in an anechoic chamber as shown in Fig. 4.2. Both far-field pattern and output power of the oscillating AIA is measured using a horn antenna which is placed 1.5 meter from the AIA. A HP 8562A spectrum analyzer is used to measure the output power of the AIA. The measured E- and H- plane radiation patterns are shown in Fig. 4.3 (a), (b), respectively. An observation of the radiation pattern shows that at broad side of AIA the cross-polarization levels is 9dB lower than co-polarization in E-plane pattern and 13dB lower in H-plane radiation pattern. This radiation pattern observation shows good agreement with that of the passive CPW-fed ZOR antenna.

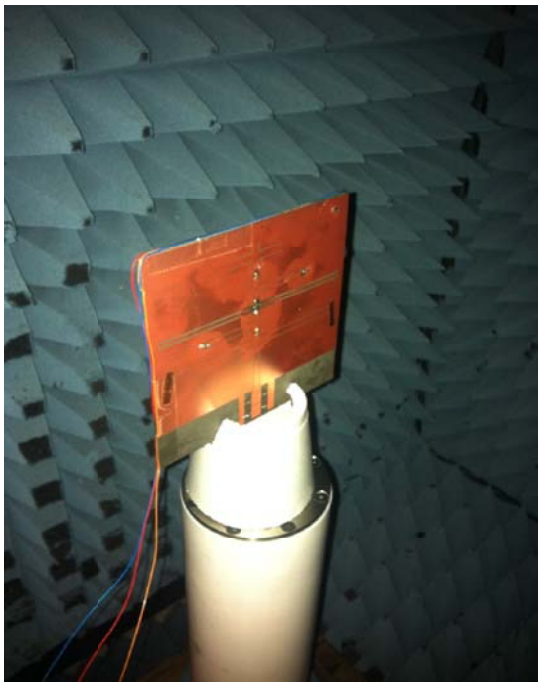

Figure 4.2: The AIA radiation pattern measurement in anechoic chamber.

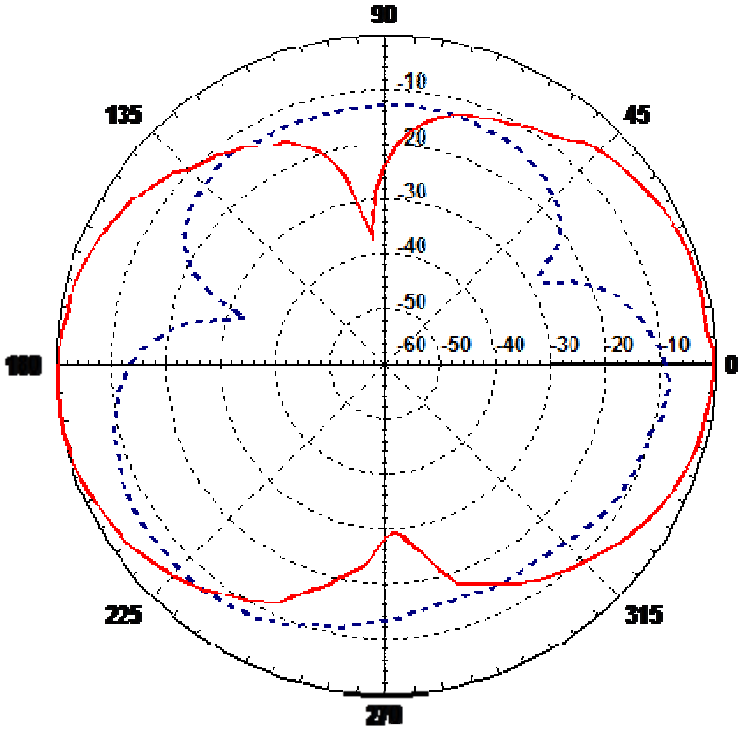

(a)

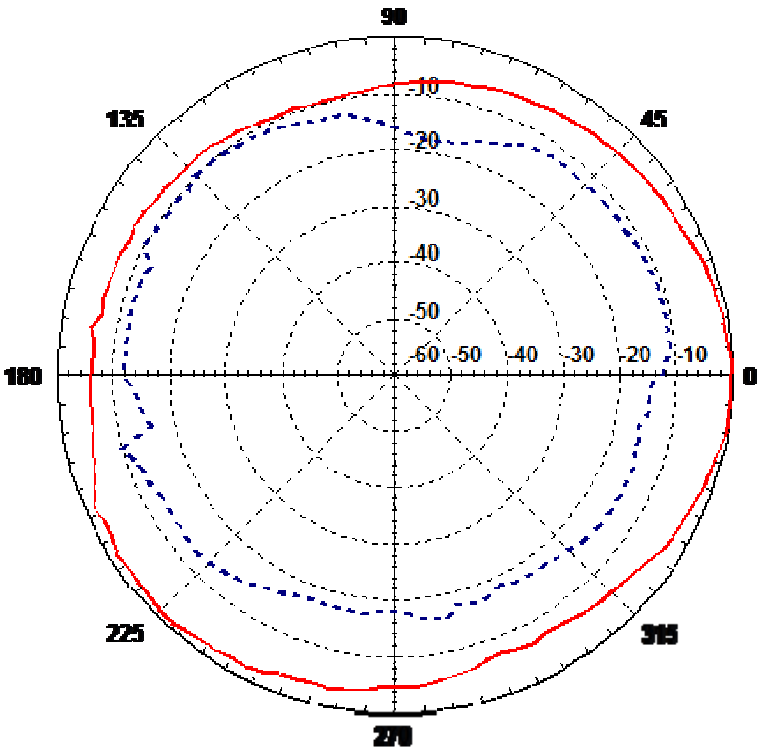

(b)

Figure 4.3: The normalized (a) E-plane and (b) H-plane radiation pattern from the oscillating AIA measurement. (Solid line represents co-polarization and dash line represents cross polarization)

Due to the high Q-factor of the electrically small ZOR antenna good phase noise performance is achieved. The phase noise is calculated by [36]

$$P_{NOISE} = P_{SIDEBAND} - P_{CARRIER} - 10\log(RBW) \tag{4.1}$$

The phase noise is estimated -92.5dBc/Hz at 100kHz offset. The radiated power of AIA and the effective isotropic radiated power (EIRP) are estimated by following process:

1. Measure a radiated power of the passive CPW-fed ZOR antenna.

   (The measurement is performed with a standard gain horn antenna at broad side. the input

power from signal generator is 10dBm at fundamental mode operating frequency.)

2. Compare the radiated power from the passive CPW-fed ZOR antenna with one from the AIA.

3. By doing the above comparison, we can also find the input power of the AIA, which can be represented as the radiated power of AIA, by comparing with the input power of the passive CPW-fed ZOR antenna. (In this case, the cable loss is taken into account to calculated the input power of the AIA.)

4. Using the passive antenna gain, assume the EIRP of the AIA for the fundamental mode frequency.

5. The second, third and fourth modes EIRP of the AIA are estimated using the same procedure above.

From the above procedure, 14.57dBm (28.64mW) of radiated power of AIA is estimated at 2.26GHz. Also, since the passive CPW-fed ZOR antenna gain is measured to be 1.54dBi, the EIRP of the AIA, is assumed 16.11dBm (40.83mW) at 2.26GHz.

The EIRP is defined as,

$$EIRP = P_t - L + G \tag{4.2}$$

where P_t is transmitted power, L is cable loss, and G is antenna gain.

The second, and third and fourth modes EIRP of the AIA are estimated to be -11.93dBm at 4.52GHz, -2.76dBm at 6.78GHz, and -17.03dBm at 9.04GHz, respectively. The experimental result shows that higher order harmonics are suppressed as it is expected in the simulation. The suppressed higher harmonic power decreases the radiation loss in the AIA. Therefore, the DC-RF power conversion efficiency is increased. Since the AIA is biased with V_{DS}=3V

and the drain DC current is measured 35mA, the DC power loss is calculated as 105mW. Therefore, the DC-RF power conversion efficiency is calculated about 27.2%, which is higher than conventional oscillating AIA [11] [12].

Chapter 5

Conclusion

In this thesis, we propose a power efficient active antenna that is integrated with an electrically small ZOR antenna using the CPW technology. The basic metamaterial concept is explained and then, ZOR antenna is introduced for the proposed AIA design. For oscillator design, the negative resistance method is introduced and employed to design the oscillator type AIA. The proposed AIA is designed using CPW technology which has many benefits such as design freedom and fabrication simplicity. The ZOR antenna is used to reduce antenna size and to obtain a good phase noise of -92.5dBc/Hz at 100kHz. A high DC-RF conversion efficiency (27.2%) is obtained by suppressing higher order harmonics and then reducing radiation loss in the AIA circuit. The proposed oscillator type AIA is electrically small and produces good radiated power 14.57dBm (28.64mW) with a high DC-RF conversion efficiency. The EIRP is calculated to be 16.11dBm (40.83mW). Therefore, the proposed AIA can be suggested as a good candidate for the spatial power combiner in array systems.

Chapter 6

Bibliography

[1] J. Lin and T. Itoh, "Active integrated antennas," *IEEE Transactions on Microwave Theory and Techniques*, Volume 42, Issue 12, Page(s):2186 - 2194, Dec. 1994.

[2] K. Chang, R.A. York, P.S. Hall and T. Itoh, \Active integrated antennas," *IEEE Transactions on Microwave Theory and Techniques,* Volume 50, Issue 3, Page(s): 937-944, Mar. 2002.

[3] A. R. Kerr, P. H. Siegel, and R. J. Mattauch, "A simple quasi-optical mixer for 100–120 GHz," in *IEEE MTT-S Int. Microwave Symp. Dig.,*Denver, CO, Page(s): 96–98, June 1977.

[4] B. Grob, *Basic Electronics*, 6 ed. New York: McGraw-Hill, 1959, ch.8.

[5] R. A. York and Z. B. Popovic´, Eds., *Active and Quasi-Optical Arrays for Solid-State Power Combining*. New York: Wiley, 1997.

[6] L. Wandinger and V. Nalbandian, "Millimeter-wave power combining using quasioptical techniques," *IEEE Trans. Microwave Theory Tech.*, Volume 31, Issue 2 Page(s):189–193, Feb. 1983.

[7] J. W. Mink, “Quasi-optical power combing of solid-state millimeter-wave sources,” *IEEE Trans. Microwave Theory Tech.*, Volume 34, Issue 2, Page(s): 273–279, Feb. 1986.

[8] S. Kawasaki and T. Itoh, “40 GHz quasi-optical second harmonic spatial power combiner using FETs and slots,” in *1992 IEEE MTT-S Int. Microwave Symp. Dig.,* Volume 3, page(s): 1543-1546 June 1992.

[9] R**.** A. York and R. C. Compton, “Quasi-optical power combining using mutually synchronized oscillator arrays,” *IEEE Trans. Microwave Theory Tech.,* Volume *39,* Issue 6, page(s): 1000-1009, June 1991.

[10] J. Birkeland and T. Itoh, “A 16-element quasi-optical FET oscillator power-combining array with external injection locking,” *IEEE Trans. Microwave Theory Tech.,* Volume 40, Issue 3, pp. 475-481, Mar. 1992.

[11] B.K. Kormanyos, W., Jr. Harokopus, L.P.B. Katehi, G.M. Rebeiz, "CPW-fed active slot antennas," *IEEE Transactions on Microwave Theory and Techniques,* Volume 42, Issue 4, Page(s):541-545, Apr. 1994.

[12] R. A. York, R. D. Martinez, and R. C. Compton, "Active patch antenna element for array application", *Electronics Letter.,* Volume 26, Issue 7, page(s): 494 - 495, July 1990.

[13] C. H. Mueller, R. Q. Lee, R. R. Romanofsky, C. L. Kory, K. M. Lambert, F. W. Van Keuls, F. A. Miranda, "Small-Size X-Band Active Integrated Antenna With Feedback Loop," IEEE Transactions on Antennas and Propagation, Volume 56, Issue 5, page(s): 1236 - 1241, May 2008.

[14] V. G. Veselago, “The electrodynamics of substances with simultaneously negative values of ε and μ,” *Sov. Phys. Usp*, vol. 10, no. 4, page(s). 509–514, Jan.–Feb. 1968.

[15] G. V. Eleftheriades, A. K. Iyer, and P. C. Kremer, “Planar negative refractive index media using periodically LC loaded transmission lines,” *IEEE Trans. Microw. Theory Tech.*, vol. 50, no. 12, page(s): 2702–2712, Dec. 2002.

[16] G. V. Eleftheriades, A. Grbic, and M. Antoniades, “Negative-refractive-index metamaterials and enabling electromagnetic applications,” in *Proc. IEEE Int. Symp. Antennas and Propag.*, Monterey, CA, vol. 2, page(s): 1399–1402. Jun. 2004

[17] G. V. Eleftheriades, “Enabling RF/microwave devices using negativerefractive-index transmission-line (NRI-TL) metamaterials,” *IEEE Antennas Propag. Mag.*, vol. 49, no. 2, page(s): 34–51, Apr. 2007.

[18] A. Sanada, C. Caloz, and T. Itoh, “Novel zeroth-order resonance in composite right/left-handed transmission line resonators,” in *Proc. Asia-Pacific Microwave Conf.*, Seoul, Korea, Nov. 2003, vol. 3, pp.1588–1592.

[19] C.-J. Lee, K. M. K. H. Leong, and T. Itoh, “Composite right/left-handed transmission line based compact resonant antennas for RF module integration,” *IEEE Transactions on Antennas Propagation*, vol. 54, pp. 2283–2291, Aug. 2006.

[20] A. Lai, K. M. K. H. Leong, and T. Itoh, “Infinite wavelength resonant antennas with monopole radiation pattern based on periodic structures,” *IEEE Transactions on Antennas and Propagation*, vol. 55, no. 3, pp. 868–875, Mar. 2007.

[21] T. Jang, J. Choi, S. Lim, "Compact Coplanar Waveguide (CPW)-Fed Zeroth-Order Resonant Antennas With Extended Bandwidth and High Efficiency on Vialess Single Layer", *IEEE Transactions on Antennas and Propagation*, vol. 59, Issue 2, page(s): 363 – 372, Feb. 2011.

[22] V. Veselago, "The electrodynamics of substances with simultaneously negative values of ε and μ," *Soviet Physics Uspekhi*, vol. 10, no. 4, pp. 509-514, Jan.-Feb. 1968.

[23] J. B. Pendry, A. J. Holden, D. J. Robbins, and W. J. Stewart, "Magnetism from conductors and enhanced nonlinear phenomena," *IEEE Trans. Microwave Theory and Techn.*, vol. 47, no. 11, pp. 2075-2084, Nov. 1999.

[24] D. R. Smith, W. J. Padilla, D .C. Vier, S. C. Nemat-Nasser, and S. Schultz, "Composite medium with simultaneously negative permeability and permittivity," *Phys. Rev. Lett.*, vol. 84, no. 18, pp. 4184-4187, May 2000.

[25] D. R. Smith and N. Kroll, "Negative refractive index in left-handed materials," *Phys. Rev. Lett.*, vol. 85, no. 14, pp. 2933-2936, Oct. 2000.

[26] R. A. Shelby, D. R. Smith, and S. Schultz, "Experimental verification of a negative index refraction," *Science*, vol. 292, pp. 77-79, Apr. 2001.

[27] C. Caloz and T. Itoh, "Electromagnetic metamaterials: Transmission line theory and microwave applications, the engineering approach," *John Wiley & Sons, New York,* 2005.

[28] C. Caloz and T. Itoh, "Transmission line approach of left-handed (LH) materials," *USNC/URSI National Radio Science meeting*, vol. 1, pp. 39, June, 2002.

[29] G. V. Eleftheriades, O. Siddiqui and A. K. Iyer, "Transmission line models for negative refractive index media and associated implementations without excess resonators," *IEEE Microwave Wireless compon. Lett.,* vol. 13, no. 2, pp. 51-53, Feb. 2002.

[30] C. Caloz, C.-C. Chang, and T. Itoh, "Full-wave verification of the fundamental

properties of left-handed materials in waveguide configurations," *Journal of Applied Physics*, vol. 90, no. 11, pp. 5483-5486, Aug. 2001.

[31] A. Lai, C. Caloz, and T. Itoh, "Composite right/left-handed transmission line meta-materials," *IEEE Microwave Magazine*, vol. 5, no. 3, pp. 34-50, Sept. 2004.

[32] David M. Pozar, "Microwave Engineering", *Wiley*, 1997.

[33] Kurokawa, K, "Some Basic Characteristics of Broadband Negative Resistance Oscillator Circuit," *Bell System Technical Journal,* Vol. 48, page: 1937–1955, July 1969.

[34] G. Gonzalez, "Foundations of Oscillator Circuit Design", *Artech House Inc.,* MA, 2007

[35] Cheng P. Wen, "Coplanar Waveguide: Surface Strip Transmission Line Suitable for Nonreciprocal Gyromagnetic Device Applications," *IEEE Trans. Microwave Theory and Techn.*, vol. MTT-17, no. 12, page: 1087-1090, Dec. 1969.

[36] Y. Cassivi and K. Wu, "Low Cost Microwave Oscillator Using Substrate Integrated Waveguide Cavity," IEEE Microwave and Wireless Components Letters. Vol. 13, no. 2, page: 48-50, Feb. 2003.